power savings are increased up to 97% in peak power and up to 99% in average power. Unlike previous approaches [3], which trade-off compression ratio and power dissipation, power savings are obtained at no cost in compression ratio. Rather, due to the new coding scheme shown in Table 1 which exploits the characteristics of low power sequences, the compression ratio is also increased up to 95% as shown in Table 2.

Conclusion: In contrast to recently published research [3] which reduces the test data volume at the expense of higher power dissipation, this Letter has shown that by using a new compression method simultaneous reduction of test data volume and power dissipation can be achieved. This research finding contributes towards development of efficient solutions for the emerging SOC testing area.

6 September 2001
Electronics Letters Online No: 20010981
DOI: 10.1049/el:20010981

P. Rosinger, P.T. Gonciari and B.M. Al-Hashimi (*Room 3053, Mountbatten Building, Highfield, Southampton, SO17 1BJ, United Kingdom*)

E-mail: p.rosinger@ecs.soton.ac.uk

N. Nicolici (*McMaster University, Communications Research Laboratory, Department of Electrical and Computer Engineering, 1280 Main St. W., Hamilton, ON L8S 4K1, Canada*)

References

1 ZORIAN, Y.: 'A distributed BIST control scheme for complex VLSI devices'. Proc. 11th IEEE VLSI Test Symp., Atlantic City, NJ, USA, 1993, pp. 4–9

2 NICOLICI, N., AL-HASHIMI, B.M., and WILLIAMS, A.C.: 'Minimisation of power dissipation during test application in full scan sequential circuits using primary input freezing', *IEE Proc., Comput. Digit. Tech.*, 2000, **147**, (5), pp. 313–322

3 CHANDRA, A., and CHAKRABARTY, K.: 'Combining low-power scan testing and test data compression for system-on-a-chip'. Proc. IEEE/ACM Design Automation Conf. (DAC), New Orleans, USA, 2001, pp. 166–169

4 DABHOLKAR, V., CHAKRAVARTY, S., POMERANZ, I., and REDDY, S.M.: 'Techniques for minimizing power dissipation in scan and combinational circuits during test application', *IEEE Trans. Comput.-Aided Des. Integr. Circuits Syst.*, 1998, **17**, (12), pp. 1325–1333

Analysis of scattering from 2D penetrable object using iterative FEM with novel mesh truncation

Jungwon Lee, Jongkuk Park and Sangwook Nam

An iterative finite element method is proposed to analyse scattering from a two dimensional penetrable object. Conventionally, to solve this kind of problem, the whole penetrable object is discretised, which is unduly costly if the object contains a large homogeneous region. By introducing a fictitious boundary inside in addition to outside the scatterer, the problem region can be greatly reduced. Also, the typical finite element method is applied with iteratively improved radiation-type boundary conditions. To validate the proposed method, a numerical example is presented.

Introduction: A variety of techniques have been proposed to solve radiation or scattering problems using the finite element method (FEM). Among them, hybrid methods such as the finite element boundary integral method (FEBIM) and methods incorporating various types of absorbing boundary conditions (ABC) have been used successfully [1]. However, each method has its inherent shortcomings. Hence, other techniques such as the FEM-based iterative method (or iterative FEM) have been suggested [2, 3]. However, early efforts using the iterative FEM incorporate the Dirichlet-type boundary condition and are prone to the well-known internal resonance problem. To overcome this drawback, new schemes which adopt the radiation-type (mixed) boundary conditions have been devised and successfully applied [4, 5].

When these various schemes are applied to analyse scattering from a penetrable object, it is common practice to discretise the whole interior region, which is unduly costly if the scatterer contains a large homogeneous region. Of course, if the scatterer is fully inhomogeneous, there is no other way than to discretise the whole interior region. But if the scatterer contains a large homogeneous part, e.g. a homogeneous dielectric object or a homogeneous dielectric object coated with another dielectric material, we can reduce the problem region greatly by introducing a fictitious boundary inside the scatterer.

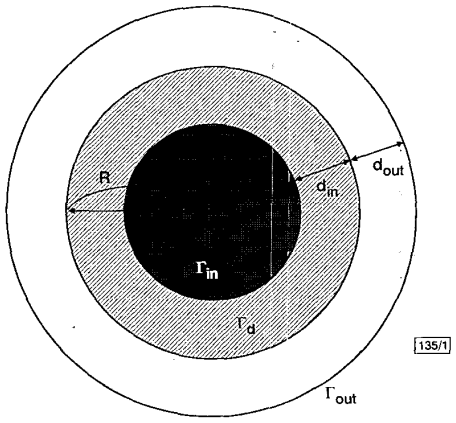

Fig. 1 *Geometry of homogeneous dielectric cylinder and two fictitious boundaries under consideration*

Theory: As an example of the proposed method, the scattering from a 2D homogeneous dielectric cylinder under E_z polarisation incidence is analysed. This method is also applicable to the inhomogeneous dielectric scatterer as long as the aforementioned property is satisfied. In this Letter, we use the iterative FEM with radiation-type boundary conditions.

Fig. 1 shows the geometry of a homogeneous dielectric cylinder and two fictitious boundaries under consideration. The shaded region is the dielectric scatterer and Γ_d is the dielectric surface. Γ_{in} and Γ_{out} are the inner and outer fictitious boundaries, respectively. Only the hatched region between Γ_{in} and Γ_{out} is discretised. In other words, the dielectric region inside the inner fictitious boundary is not meshed. Hence, the problem size can be greatly reduced.

For the E_z polarisation case, the field E_z in the source-free region satisfies the scalar Helmholtz equation

$$\nabla^2 E_z + k_0^2 \varepsilon_r E_z = 0 \tag{1}$$

and the boundary conditions are given by

$$\frac{\partial E_z}{\partial n} + jk_d E_z = \psi_{in} \quad \text{on} \quad \Gamma_{in} \tag{2}$$

$$\frac{\partial E_z}{\partial n} + jk_0 E_z = \psi_{out} \quad \text{on} \quad \Gamma_{out} \tag{3}$$

where $\partial/\partial n$ is the derivative with respect to the outward normal. The choice of the boundary conditions require some reasoning. In general, the Sommerfeld radiation condition is satisfied in the far field region as follows:

$$\lim_{\rho \to \infty} \sqrt{\rho}\left(\frac{\partial E_z}{\partial \rho} + jk_0 E_z\right) = 0 \tag{4}$$

Since the fictitious boundaries Γ_{in} and Γ_{out}, where the mesh is terminated, are placed near the scatterer, the Sommerfeld radiation condition is not valid and the boundary conditions must be reconstructed as described previously. These radiation-type mixed boundary conditions mean that the left side of the Sommerfeld radiation condition does not vanish in the near field region. The key idea in this Letter is based on the update of these residual terms in Γ_{in} as well as Γ_{out} which is different from the conventional iterative FEM. With these radiation-type boundary conditions, the functional is given as follows [1]:

$$F(E_z) = \frac{1}{2}\iint_{\Omega}\left[\left(\frac{\partial E_z}{\partial x}\right)^2 + \left(\frac{\partial E_z}{\partial y}\right)^2 - k^2 E_z^2\right] d\Omega + \int_{\Gamma_{out}}\left(\frac{jk_0}{2}E_z^2 - \psi_{out}E_z\right) d\Gamma + \int_{\Gamma_{in}}\left(\frac{jk_d}{2}E_z^2 - \psi_{in}E_z\right) d\Gamma \quad (5)$$

Initially, ψ_{in} and ψ_{out} are calculated with an assumption that E_z in eqns. 2 and 3 is the same as the incident electric field $E_{z,inc}$. Hence $\psi_{in} = 0$ initially. According to the typical FEM procedure, the electric fields can be determined everywhere. From these calculated fields, the equivalent electric and magnetic current sources on the dielectric surface Γ_d are introduced using the equivalence theorem. These sources then generate the fields on the fictitious boundaries, which can be calculated using the Green's function. Since these generated fields are scattered fields, the total fields on the boundaries are the sum of these scattered fields and the incident fields. In this way, the fields on the fictitious boundaries are updated, which means the update of the residual terms ψ_{in} and ψ_{out}. Through several iterations of this procedure, the fields converge to an exact solution regardless of the initial guess about ψ_{in} and ψ_{out}. Moreover, this procedure is free from the internal resonance problem since the radiation-type boundary conditions are used.

Since the system matrix generated by typical FEM is sparse and unchanged during the iterations, the computational efficiency can be greatly enhanced in this procedure.

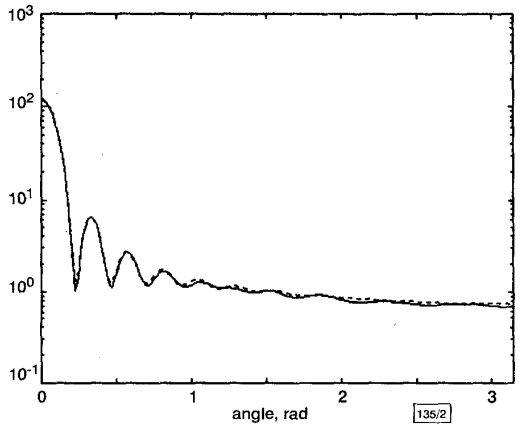

Fig. 2 *Bistatic RCS patterns for homogeneous dielectric cylinder with radius $R = 2\lambda$ and dielectric constant $\varepsilon_r = 4 - j$ under E_z polarisation incidence*

$d_{in} = d_{out} = 0.1\lambda$
——— proposed method
– – – – series solution

Numerical results: To show the validity of this method, the scattering from a 2D homogeneous dielectric cylinder under E_z polarisation incidence is analysed. The radius of the dielectric cylinder (R) is 2λ, where λ is the free space wavelength, and the dielectric constant is $4 - j$. The distances (d_{in} and d_{out}) between the dielectric surface and the fictitious boundaries are both 0.1λ. Fig. 2 shows the results obtained by the proposed method, compared with the exact solution using the series expansion. The results are in good agreement.

Acknowledgment: This work was supported by the Brain Korea 21 Project.

9 August 2001
Electronics Letters Online No: 20010986
DOI: 10.1049/el:20010986

Jungwon Lee, Jongkuk Park and Sangwook Nam (*Applied Electromagnetics Lab. (#010), Institute of New Media & Communications, School of Electrical Engineering and Computer Science, Seoul National University, San 56-1, Shinlim-dong, Kwanak-ku, Seoul 151-742, Korea*)

E-mail: ljw@inmac3.snu.ac.kr

References

1 JIN, J.M.: 'The finite element method in electromagnetics' (Wiley, New York, 1993)
2 ROY, T., SARKAR, T.K., DJORDJEVIC, A.R., and SALAZA, M.: 'A hybrid method solution of scattering by conducting cylinders (TM case)', *IEEE Trans. Microw. Theory Tech.*, 1996, **MTT-44**, (12), pp. 2145–2151
3 PARK, J., CHAE, H., and NAM, S.: 'Efficient hybrid method for characterisation of arbitrary-shaped discontinuities in a rectangular waveguide', *Electron. Lett.*, 1999, **35**, (14), pp. 1170–1171
4 ALFONZETTI, S., BORZI, G., and SALERNO, N.: 'Iteratively-improved Robin boundary conditions for the finite element solution of scattering problems in unbounded domains', *Int. J. Numer. Methods Eng.*, 1998, **42**, pp. 601–629
5 PARK, J., CHAE, H., and NAM, S.: 'Study of efficient FEM-based iteration method for open region problem and its application to scattering from three dimensional cavity-backed aperture', *Electron. Lett.*, 2000, **36**, (18), pp. 1529–1530

Broadband Raman gain characterisation in various optical fibres

F. Koch, S.A.E. Lewis, S.V. Chernikov and J.R. Taylor

The Raman gain coefficient of several different types of optical fibres has been quantified using a sensitive technique based upon the measurement of backward amplified spontaneous emission. Spectral measurement of the effect of the variation of germanium doping in the fibre is also reported.

Stimulated Raman scattering is poised to play an important role in near-term upgrading of the capacity of optical communication systems, both from a positive and negative perspective. In dense wavelength division multiplexed schemes, inter-channel stimulated Raman scattering, as a result of crosstalk, will be a potential source of noise in the system and give rise to gain tilt [1]. However, stimulated Raman based amplifiers both in lumped and in distributed format are undoubtedly perceived as key elements in the technology of system upgrade [2] through bandwidth enhancement [3, 4] or through extending the reach of amplifier spans [5]. Consequently, a detailed, quantitative characterisation of the Raman coefficient and profile of various readily and commercially available fibre types is required, if accurate modelling of the above effects are to be undertaken. Although previous studies have been undertaken [6 – 8], limited spectral resolution has restricted the subtle effects on the Raman spectral gain profile of for example germanium (Ge) content. In this Letter we illustrate the fine structural differences for different Ge dopant levels in several 'standard' fibres, measuring the Raman gain coefficient over more than 30 THz and providing an estimation of the relation between maximum gain and dopant level.

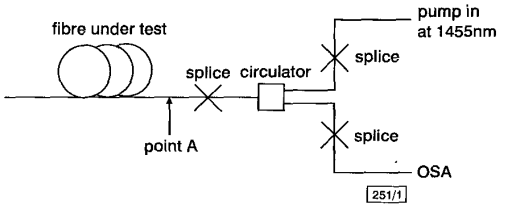

Fig. 1 *Schematic diagram of experimental configuration*

The technique used to determine the Raman gain coefficient was based on the measurement of the amplified spontaneous emission (ASE) along the test fibre [9], pumped by a narrow linewidth, high power, CW fibre Raman laser [10] at 1455 nm. In excess of 1 W was available for launch into the test fibres. Fig. 1 shows a schematic diagram of the experimental configuration, where the back scattered ASE was detected such that problems of simultaneous detection of the pump signal in close proximity to the ASE signal were negated. The simple yet highly sensitive configuration, deploying watt level CW pumping, allowed high-resolution measurement of the Raman gain profile to beyond 1000 cm^{-1} shift and